Expertise
and insight
for the future

Daniel Fasel

Hand Position and Movement Acquisition System for a Wrist Based HMI

Helsinki Metropolia University of Applied Sciences

Bachelor of Engineering

Electronics

Thesis

25 May 2021

Author(s) Title Number of Pages Date	Daniel Fasel Hand Position and Movement Acquisition System for a Wrist Based HMI 41 pages + 2 appendices 25 May 2021
Degree	Bachelor of Engineering
Degree Programme	Electronics
Professional Major	
Instructor(s)	Matti Fisher, Principal Lecturer Heikki Valmu, Principal Lecturer

The field of human-machine interfaces keeps evolving at a steady pace. In recent years gesture recognition has become an important focus of research. Most commercial applications of gesture recognition work with the help of cameras. These suffer from occlusion and low portability. Wrist based systems do not suffer from these problems, making them ideal for use cases such as translating sign language.

Current research on wrist based devices rely on neural networks to recognise the gestures. They mostly use an arbitrary set of gesture to label their data. This limits the applications of such devices as the fine movements of the hand cannot be classified by the neural networks. Any additional gesture also requires new training that is bound to the sensors used. A real-time hand position and movement acquisition system was developed in this work to improve the labeling of sensor data. With such a system researchers can create a neural network that uses the exact position of the hand instead of an arbitrary set of gestures. This device takes the shape of a 3D printed exoskeleton placed on the back of the hand. Potentiometers are used to measure the angle of each joint of the hand.

The exoskeleton has good anatomical fidelity, is affordable and easy to build. The one sigma standard deviation of the measurement accuracy is 3.1 degrees. This relatively poor accuracy is due to the potentiomteters. Individual calibration of the sensors could improve this result. This work demonstrates that using 3D printing and potentiometers is a viable solution to capture the position of the hand in real-time.

Keywords	Gesture Recognition, 3D Printing, Exoskeleton, Wristband, Position Acquisition System, Neural Network

Contents

Appendices

List of Abbreviations

ABS	Acrylonitrile Butadiene Styrene.
ADC	Analog-to-digital converter.
CAD	Computer-aided design.
CB	Carpal bones.
CMC	Carpalmetacarpal.
CNC	Computer Numerical Control.
DIP	Distal Interphalangeal.
DP	Distal phalanx.
HMI	Human-Machine Interface.
IC	Integrated Circuit.
IMU	Inertial Measurement System.
IP	Interphalangeal.
KDE	Kernel Density Estimation.
LED	Light Emitting Diode.
MB	Metacarpal bones.
MCP	Metacarpophalangeal.
MP	Middle phalanx.
PCB	Printed Circuit Board.
PETG	Polyethylene Terephthalate Glycol.
PIP	Proximal Interphalangeal.
PLA	Polylactic Acid.
PP	Proximal phalanx.

1 Introduction

Over the last half-century, the field of electronics has seen intense development. With each new generation of devices came a new Human-Machine Interface (HMI). From batch processing, terminal commands or graphical user interfaces, all the way to graspable user interfaces such as joysticks and touch screens. One area that is increasingly researched, helped by the advent of neural networks is gesture recognition. Many gesture recognition systems currently available rely on cameras to function. Compared to those systems a wrist based recognition system has multiple advantages. It is more portable and does not suffer from occlusion or low light situations. In addition to these reasons, the rise in popularity of smartwatches suggests that a wrist based system has a better form factor. As a result, this thesis work focuses on a gesture based HMI located on the wrist.

In order to develop a gesture recognition wristband, a neural network is an essential component. Such an algorithm requires two inputs. The first input is the values from the sensors located on the wrist. The algorithm then makes an estimate of the position of the hand based on this input. The second input is the actual position of the hand and is used to control the accuracy of the algorithm allowing it to ”learn”. The algorithm tunes its own variables to reduce the difference between the estimate of the position based on the sensors and the actual position of the hand.

A literature review of wrist based HMIs revealed two interesting aspects. Firstly, researchers usually use a limited set of gestures or arbitrary finger flexion to label their data instead of the real-time position of each hand joint. This means that any neural network using this control data will only be able to recognize the gestures found within the data. Any additional gestures will require more work and it is not possible to accurately detect the position of the hand joints. This approach restricts the use of the device. For example, in order to use the wristband for virtual reality simple gestures are not sufficient. Secondly, only one sensor is usually used at a time instead of a combination of different sensors. According to some research, sensor information can overlap and therefore give better results [1]. Trying different combinations of sensors would be a beneficial step.

Developing a wrist based HMI with multiple sensors and a real-time position acquisition system to acquire the control data would exceed the scope of this work. As a consequence, the goal of this thesis work was to create a position and movement acquisition system. Such a device would allow researchers to label their sensor data with the actual position of the hand instead of an arbitrary small set of gestures. The aim of the system is to provide an anatomically accurate model of the hand in real time. The difference between the true angle of a hand joint and the measured value should be less than one degree. In statistical terms this would equate to a standard deviation of 0.15°. It also needs to be affordable, easy to build and require little maintenance as it is meant for a research environment and not a commercial one. It also needs to be comfortable to wear for a longer period of time. This is to guarantee that enough data can be gathered without issues in case the algorithms require it.

2 Hand Anatomy and Motion

An understanding of the hand anatomy is a prerequisite to understand the work of this thesis. While the simple observation of our own hand suffices to follow the reasoning developed throughout this thesis, a more detailed insight of the hand anatomy and biomechanic is beneficial and will therefore be explored in this chapter.

The hand, like all parts of the human body, is not a simple topic. The purpose of this work is to transcribe the movement and position of the hand into a digital form. Therefore the focus of this chapter will be narrowed down to understanding the range of motion of the hand and how it moves. An intricate understanding of what powers the motion or the detailed hand construction is not necessary for the scope of this thesis work. The natural range of motion of the hand is constraint by multiple elements such as the bones, ligaments or joint capsules, etc. The bones prevent any movement along their length, as they are rigid bodies. This fact allows us to simplify the hand structure to a collection of bones linked together via joints. A description of the motion of these joints is therefore equivalent to a description of the hand's motion.

When talking about the range of movement for a specific joint, there is a distinction to make between a passive movement and an active movement, differentiated by the involvement of muscles. For example, when pushing a door open, the fingers can bend back further than would be possible through simple muscle contraction. For this reason the exoskeleton needs to take into account the passive range of movement and cannot be simplified to the active one. Consequently, all the ranges of freedom described below are passive.

In accordance to the simplified structure described above, the hand can be split into three parts. As illustrated in figure 1, the first part consists of the fingers, whose bones are called phalanges. Each finger, with the exception of the thumb, is made of a Distal phalanx (DP), a Middle phalanx (MP) and a Proximal phalanx (PP). The thumb is missing the MP. The second part consists of the palm of the hand, which is made of the Metacarpal bones (MB). The last part is the wrist, which is formed by eight Carpal bones (CB).

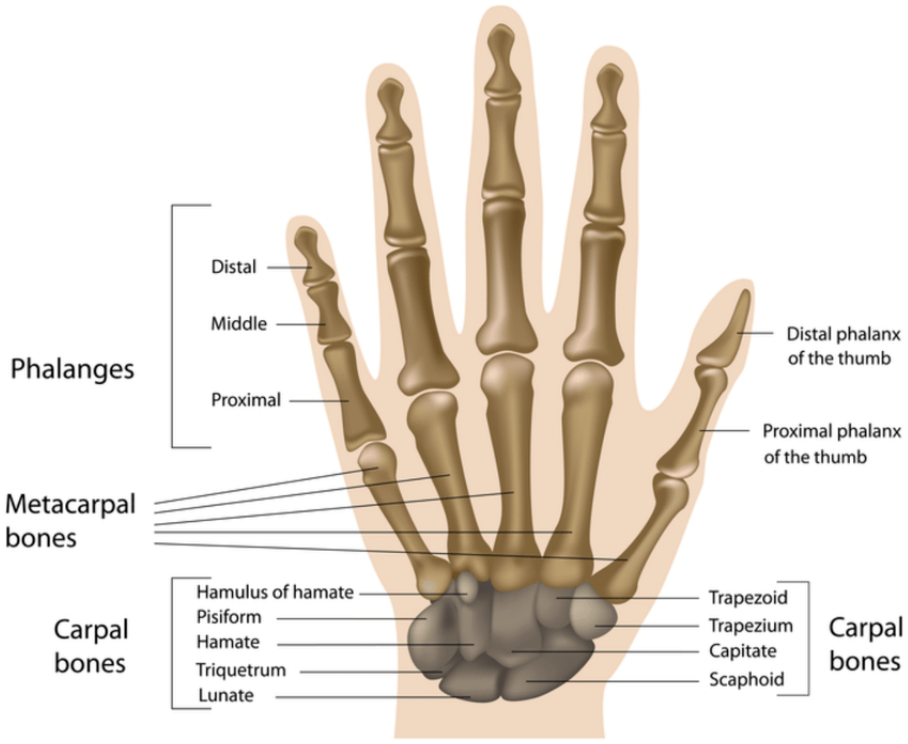

Figure 1: Bones of a human hand. Copied from Iglocikov V. [2, 2]

2.1 Finger Motion

As mentioned above and illustrated in figure 1, the fingers are formed by three phalanges. Starting from the tip of the finger, the first joint, connecting the DP and the MP, is called the Distal Interphalangeal (DIP) joint. This joint has functionally only one degree of freedom, flexion and extension. Flexion occurs when the angle between the bones is decreased while extension is the opposite, in other word it straightens the joint. Some minimal rotation is possible due to the shape of the bone endings forming the joint. Adduction and abduction, in this context a left-right movement, is also possible but as with the rotation it is negligible. As can be seen in figure 2 c, the DIP joint allows for 90° of flexion and 30° of extension. The next joint, between the MP and the PP is called the Proximal Interphalangeal (PIP) joint. Similar to the DIP joint it is a hinge joint. Hence it allows for flexion, extension and only negligible levels of rotation, adduction and abduction. As can be seen in figure 2 this joint allows for 130° of flexion but 0° of extension. [3, 66-75.]

The final finger joint is the Metacarpophalangeal (MCP) joint. Also commonly known as the knuckle joint, it has two degrees of freedom. Flexion - extension as well as adduction - abduction. In figure 2 a the range of motion of this joint is displayed. It allows for 90° of

flexion, 40° of extension and 30° of adduction - abduction. When the fingers are flexed abduction or adduction is not possible anymore. Some small rotations also occur during the flexion. The index MCP joint medially rotates when flexed (towards the middle) while the other fingers rotate laterally (towards the outside) when flexed. These rotations, as well as the abduction - adduction and rotation of the DIP and PIP joints, are important for gripping and precision movements. Though due to the complexity of measuring those small movements accurately and the small benefits gained from modeling them, they will be ignored. These rotations are also mostly correlated to other finger movements and could therefore be estimated analytically. [3, 66-75.]

These rotations are not the only aspect of the fingers and the hand helping the grasping gestures and fine movements. The shape of the palm, for example, is not flat but curved towards the inside. This is furthered pronounced with the possible movement between 5th and 4th metacarpal bones to increase the curvature of the palm. This motion will be measured as it can happen independently of any other hand motion and is easy to measure. [3, 60-62.]

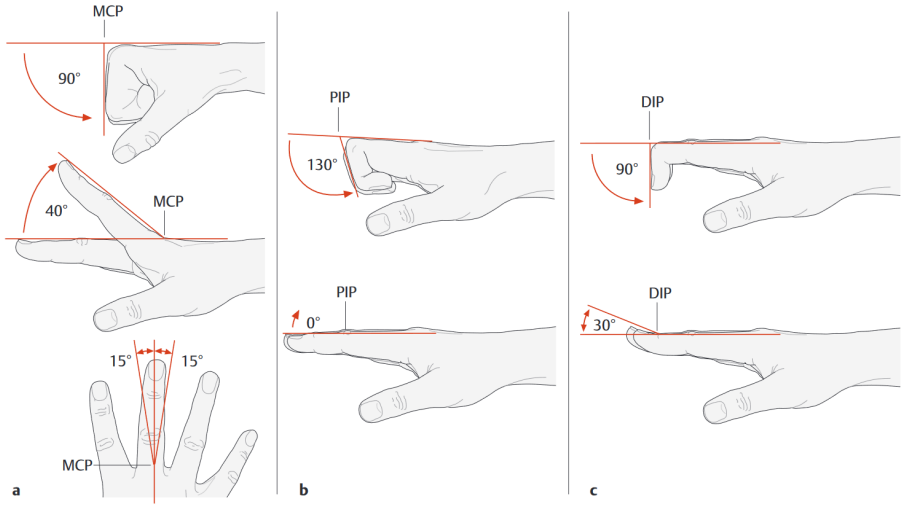

Figure 2: Motion of the phalanges. Copied from Hirt et al. [3, 75]

2.2 Thumb Motion

The thumb is arguably the most important part of the hand as is illustrated by this quote from John Napier:

> The hand without a thumb is at worst nothing but an animated spatula and at best a pair of forceps whose points don't meet properly. - John Napier (1993) [4, 380].

The first joint, starting from the tip, is a simple hinge joints. As is the case with the fingers, it allows mostly for flexion and extension. In the case of the thumb, the joints are somewhat shifted due to the missing MP. Consequently, the first joint, between the DP and the PP, is called the Interphalangeal (IP) joint. It allows for 90° of flexion and 30° of extension. The second joint, between the PP and the MB is the MCP joint. It is an ovoid joint and has two degrees of freedom. Its range of motion is 80° of flexion, 0° of extension, 12° of abduction and 7° of adduction. Some rotation is also present in those two joints but it will not be take into account in this thesis work. [3, 59-60.]

The third and last joint of the thumb, between the CB and the MB, is called the Carpal-metacarpal (CMC) joint. The uniqueness of the thumb stems from it. It is a saddle joint which gives it three degrees of freedom compared to the two degrees of freedom of the other thumb joints. In addition to the third degree of freedom, it is also attached to the CB at a 45 degree angle. [3, 49.]

As illustrated in figure 3, the first degree of freedom is called abduction and adduction. Abduction, in this case, can be described as the following motion: going from a facing up open palm gesture with the thumb tucked next to it to the thumb pointing straight up to the stars. Adduction is to opposite movement and can be visualized as ”adding” the thumb to the open palm. The CMC joint allows for 25° of adduction and 35° of abduction, the flat open palm being the rest position. The second degree is extension and flexion. In the case of the CMC joint, the movement can be described as going from a hitchhiker gesture with an open palm to the gesture representing the number four in the western world and China. This movement is described in figure 3. The range of movement is 45° of extension and 25° of flexion with the rest position being parallel to the index finger. Finally, the third degree of freedom is pronation. It consists of a rotation of the thumb when going from an open palm gesture to a gesture where the thumb and little finger touch. In combination with the small rotation of the fingers it is what makes the hands of primates excellent at grasping objects. Similarly to the other rotations of the fingers, it is quite limited and happens synchronously with the two other movements. Therefore, it was not measured for this thesis work. [3, 48-49.]

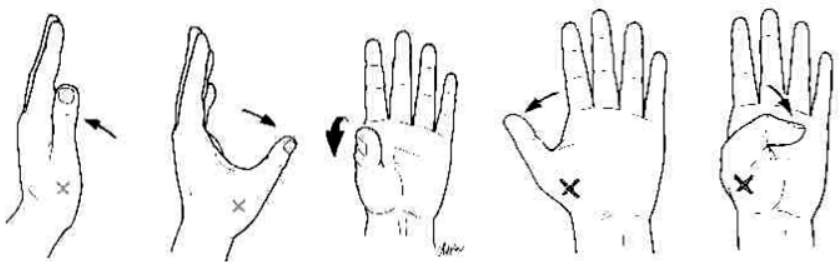

Figure 3: Motion of the thumb. Copied from Rahman and Al-Jumaily [5, 49]

2.3 Wrist Motion

The wrist is the most complex joint of the hand as it consists of 8 different bones. In reality these 8 bones form two separate joints that work together to move the wrist. For the purpose of this thesis work, the model of the wrist can be simplified to a single joint with two degrees of freedom. There is flexion - extension and radial - ulnar deviation. As shown by figure 4 the radial and ulnar deviation can be described as a left-to-right movement. The combined joints forming the wrist allow for approximately 80° of flexion as well as extension, between 15° and 25° of radial deviation and around 40° to 50° of ulnar deviation. [3, 15.]

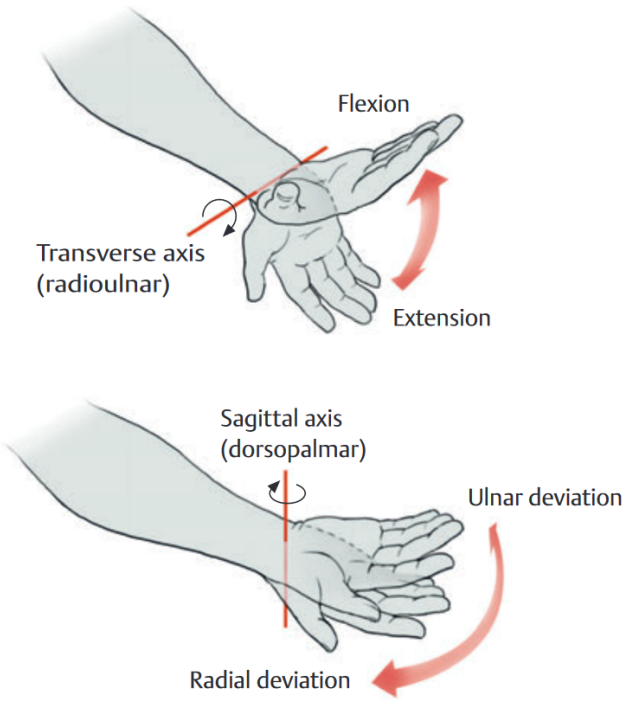

Figure 4: Motion of the wrist. Copied from Hirt et al. [3, 11]

3 Sensor Circuitry

A system that transcribes a real world phenomena into a digital variable requires a sensor. In this thesis, the following definition for sensor is used:

> Sensor: a device that responds to a physical stimulus (such as heat, light, sound, pressure, magnetism, or a particular motion) and transmits a resulting impulse (as for measurement or operating a control). [6]

In electronics the resulting impulse is in the form of an electric signal. Electronic sensors work in a multitude of ways and may contain multiple stages before converting the signal to an electric signal. For example, an optical mouse does not transcribe the displacement directly into an electric signal. Instead, it illuminates the surface underneath it with a laser or a Light Emitting Diode (LED). The light then bounces off the surface and impacts an array of light detectors, representing the pixels. These detectors transform the colliding photons into an electric current in order to form a digital image. Finally, the image is compared to the previous image which allows for the displacement of the mouse to be measured. [7, 313-314.]
When looking at the sensors that directly transform a physical stimulus to an electric signal, six main types can be distinguished [7]:

- Electric Field Sensors
- Magnetic Sensors
- Capacitive Sensors
- Resistive Sensors
- Piezoelectric Sensor
- Photoelectric Sensor

Some of these types can be used to measure different physical properties. For example, a resistive sensor measures the change in resistance and this change can occur for multiple reason such as temperature, humidity, stretching, etc. The opposite is also true, a physical

property can be measured with different sensor types. In the case of temperature one can find photoelectric sensors, resistive sensors, capacitive sensors, etc.

The sensors required by this thesis work are angle sensors. As with temperature, there are multiple sensors of different types that can measure angles. The process through which the sensors were chosen and the circuitry resulting from this choice will be described in the following chapters.

3.1 Joint Angle Sensors

As mentioned above, there are a considerable number of sensors that can measure angles directly or indirectly. Going through all the different possibilities and selecting the best candidate is not feasible due to this vast selection. As an example, while impractical, it is possible to measure an angle with a temperature sensor. Placing a candle at the end of a slider crank mechanism, with a thermometer on the other end, will link the rise in temperature to a rotation of the crank, in other words, a change in angle. Due to this, certain criteria have been chosen to narrow down the options. The candidates were selected by looking at the sensors used in similar works and by searching the internet for the most commonly used angle sensors. This was done to ensure that the found options are readily available without missing out on some sensors that would be uncommon but specifically suitable for this use case.

Five sensing methods were found through this method. When looking at generic angle sensors, potentiometers and rotary encoders stand out. Looking at similar projects to this thesis work four sensors stand out. Ultrasound sensors [8], an Inertial Measurement System (IMU) [9], cameras [10] and finally a flex sensor [11].

While all the sensors above can measure angles, this project has specific requirements that makes some sensor more usable than others. The device should be affordable and easy to use. The sensors used in similar projects fail these requirements. The IMU, rotary encoder as well as the flex sensors are too expensive as they cost above 10 euros per sensor at the time of this writing. The cameras and the ultrasound sensors, while relatively affordable, suffer from occlusion. In other words, the hand can sometimes be hidden from the sensors which then lose track of its position. This leaves the potentiometers as the

most suitable choice.

There is a plethora of potentiometers to choose from. In this context, aside from the price and accuracy, the most important aspect is the form factor. The range of motion of the hand, described in chapter 2, dictates the placement of the potentiometers. In order to not hinder the movements, they need to be placed on the back of the hand and fingers. This severely limits the size of the potentiometers since they need to fit on top of the little finger MP. With this size constraints, surface mounted potentiometers were the only available option. Finally, the choice was made to use a $10K\Omega$ surface mounted SV03A103 potentiometer from Murata, illustrated in figure 5.

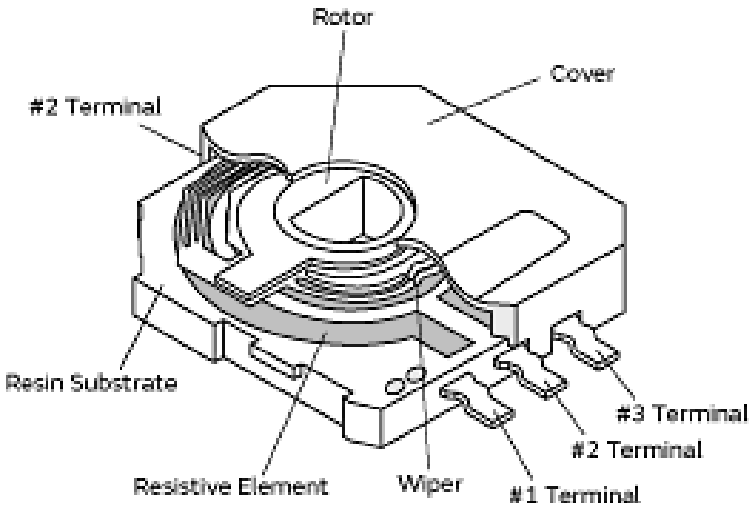

Figure 5: SV03A103 from Murata, copied from its datasheet. [12]

A potentiometer functions as two resistors in series. The combined resistance, formed by a resistive element, is the resistance of the potentiometer. A wiper contacts the resistive element and separates it into the two resistors. The position of the wiper determines the resistance ratio between the two sides of the resistive element. By calculating the voltage between the viper and ground (or power), the position of the wiper can be found. In the case of the SV03A103, as can be seen in figure 5, the terminals one and three are respectively the power and ground and are interchangeable. The terminal two is connected to the wiper and is used to measure the angle of the potentiometer.

As described in the previous chapter, our hand is comprised of over 16 joints. Some have more than one degree of freedom and therefore require more than one potentiometer.

Four sensors per finger were used and two for the thumb. In addition to this, three sensors were used for the thumb-wrist joint, one sensor for the flexion between the 4th and 5th metacarpal bones and two sensors for the wrist joint. This amounts to a total of 24 sensors. Each sensor requires three wires which means that 72 wires would have to be brought from the wrist to the microcontroller, in this case, an Arduino Nano 33 BLE. This number of wires could cause signal noise as well as physically hinder certain movements. To alleviate these problems, a wire combining Printed Circuit Board (PCB) was created to limit the number of wires.

3.2 Wire Combining Circuit

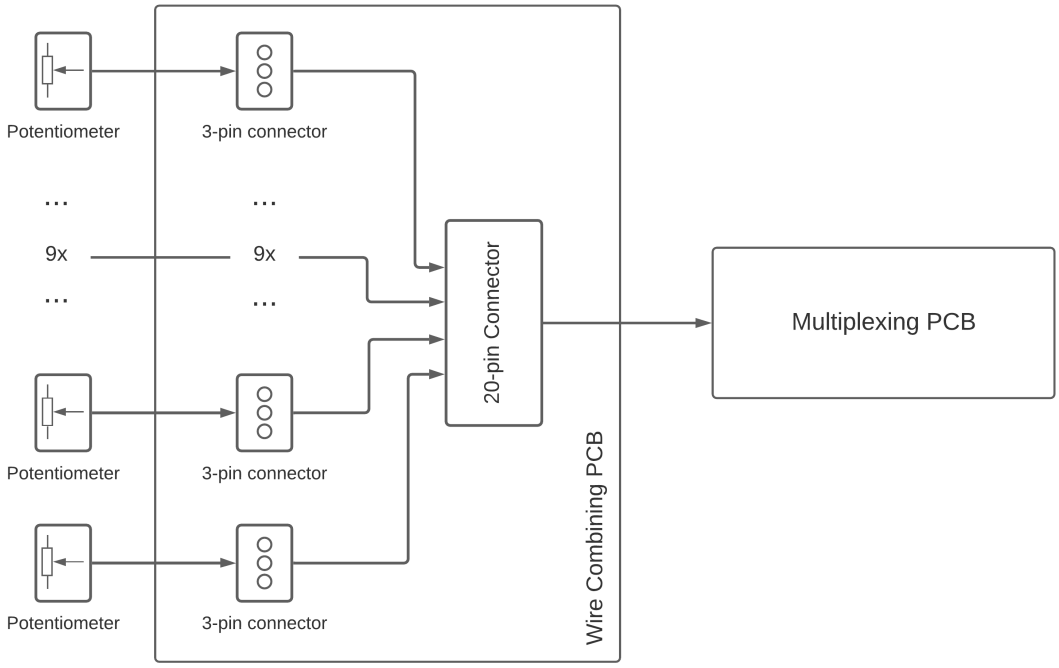

Figure 6: Flow chart of the wire combining PCB.

In order to prevent 72 wires from traveling above the wrist, a PCB was designed that combines the ground and power wires from the sensors. A flowchart of the design can be seen in figure 6 and the final schematic can be found in appendix 2.1. The board reduces the number of wires from 74 to 40. Due to the small size of the hand, the circuit is designed to have two identical PCB's stacked on top of each other. Each potentiometer is connected to the board via connectors denoted in the schematic by the reference designators J1 to J12. From there the grounds and powers of the potentiometers are combined while the signal wires are routed to a 2X10 connector (J13). The board additionally houses 10

uF capacitors between power and ground (C13,C14) and 2.7 nF capacitors between the signal wires and ground (C1-C12). These capacitors are there to reduce noise in the signal.

The value of the signal to ground capacitors was chosen while paying attention that a 120 Hz sampling rate remains possible as too much capacitance can cause lag. The potentiometers are all in parallel which means that equation (1) can be used to calculate the total resistance.

$$\frac{1}{R_{Total}} = \frac{1}{R_1} + \frac{1}{R_2} + \frac{1}{R_3} + ... + \frac{1}{R_n} \tag{1}$$

The resulting total resistance is 417Ω. With the resistance and the voltage known (3.3 V), it is possible to calculate the time constant τ of the capacitor given by equation (2).

$$\tau = R \cdot C = \frac{1}{2\pi f_c} \tag{2}$$

This constant indicates how much of the capacitor is charged after the calculated time. One time constant equates to 63%, two time constants to 86.5% and three time constants to 95% [7, 51]. While the capacitor is charging, the current is not flowing all the way to the Analog-to-digital converter (ADC) that will measure the signal but is ”captured” by the capacitor. This signifies that any signal change that is faster than the charging of the capacitor will not be measured and will simply be absorbed by the capacitor introducing lag in the measurement. With a 120 Hz sampling rate one sample is taken every $\frac{1}{120} = 0.0083$ seconds. There are two capacitors in parallel for each signal as there is an additional capacitor on the multiplexing PCB which will be described in the chapter 3.3. According to this, equation (3) can be used to calculate the maximum capacitance permitted so that 95% of the capacitor gets charged within the available time.

$$C = \frac{\tau}{R} \tag{3}$$

The resulting capacitance is 21.2 [µF], given by equation (4).

$$\frac{0.008\overline{3}}{416.\overline{6}} = 0.0000212[F] \tag{4}$$

The capacitors were supposed to be 2.7 μF but due to a mistake 2.7 nF capacitors were

ordered. An additional capacitor between signal and ground is located on the multiplexing PCB, described in the next chapter. This would make the total capacitance 5.4 μF which is well below the maximum value allowed. The ordered capacitors are 1000 times smaller making this problem irrelevant.

3.3 Multiplexing Circuit

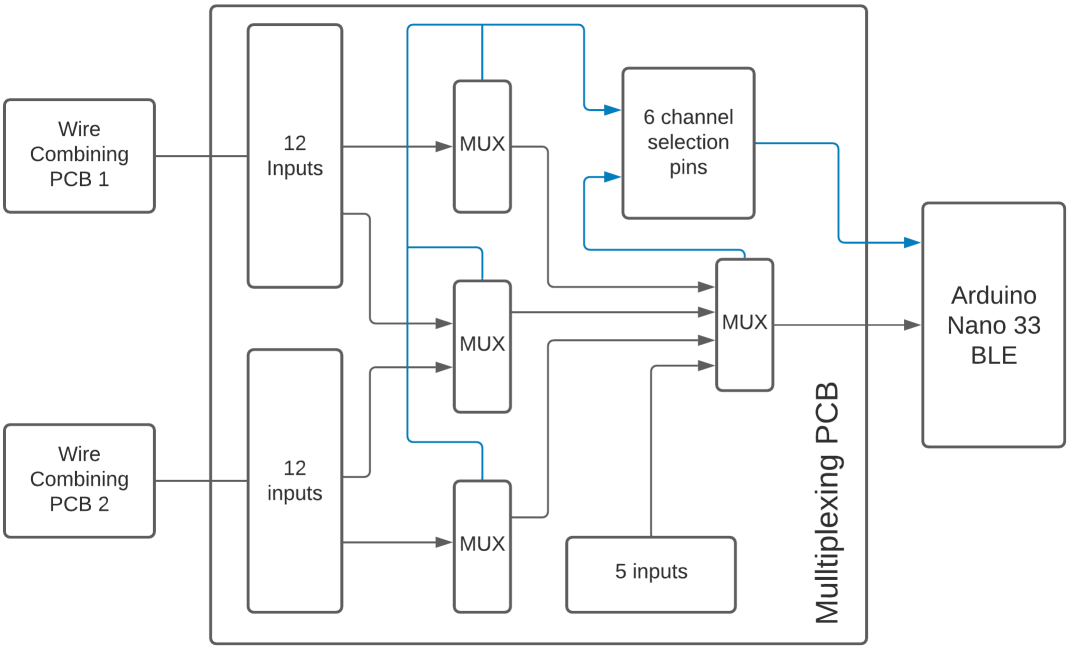

Figure 7: Flow chart of the multiplexing PCB.

The next problem caused by the large number of sensors is at the microcontroller level. A typical microcontroller has only a limited number of analog pins, eight in the case of the Arduino Nano 33 BLE. This means that a multiplexing circuit needs to be designed to reduce the number of pins required to read the data from the sensors. A simplified description of the board circuitry can be seen in figure 7 while its complete schematic can be found in appendix 2.2. The board contains four cascaded multiplexers. A multiplexer is a device that has multiple inputs, eight in this case, and one output. The input channel is then selected through a binary combination. On the board, three multiplexers have connected selection pins. Their output goes to the fourth multiplexer whose selection pins are independent from the other multiplexers. The design originally contained a buffer through which the output signal goes. This is to be sure that the input resistance of the ADC does not affect the readings. After testing, it turned out that this was not an issue

and the buffer was removed. During testing it also became apparent that cascading the multiplexers causes issues. The reason for it was not found and as a temporary solution the output wires of the first three multiplexers were connected directly to the Arduino. Capacitors were also used, as in the wire combiner PCB, to smooth the signal and stabilize the power and ground. Additionally, each multiplexer has a decoupling capacitor that is also there to ensure a stable supply voltage to the Integrated Circuit (IC). Finally the analog and digital signals were separated in the design to reduce noise.

4 Hand Exoskeleton

Potentiometers were chosen as the sensors of this project. As a consequence, some physical construct was needed to hold the chosen potentiometers in place and rotate them synchronously with the joints. As previously explained, the only place for such a construct is on the back of the hand, as it remains unobstructed for the full range of motion of the hand. Being on the back of the hand the construct will take the shape of an exoskeleton. Exoskeleton coming from the Greek words exo- (outside) [13, p.160] and skeleton [13, p.441]. This exoskeleton also needs to accommodate the wire combining PCB described in chapter 3.2. The most common implementations of exoskeletons in the engineering world are powered and are used to augment the ability of the wearer. In this case there are no motors but only sensor, as the purpose is only to detect the position of the hand. This makes the construction less demanding and opens the possibilities for different construction methods. The design and construction process of this exoskeleton will be described in this chapter.

4.1 Materials and Manufacturing Method

This hand position and movement acquisition system is intended to gather data to train a neural network. Therefore, it is mainly intended to be used for research purposes and consequently should be cheap and easy to build. With these criteria in mind, the first step is to select the materials and their related manufacturing method. Small, yet functional pieces have certain material requirements and most metals and plastics fulfil those requirements. This leaves the manufacturing method as the deciding factor. Working with metal requires a specific skill set and/or expensive tools such as a Computer Numerical Control (CNC) machine or a lathe. On the other hand, using plastic benefits from the advent of 3D printers. In recent years they have become readily available in schools, and even libraries. Being so affordable and compact it is even conceivable to purchase one for personal use. This price difference and ease of use makes 3D printing the manufacturing method of choice for this thesis work.

There is a large variety of plastic used by 3D printers. Some common ones are Polylactic Acid (PLA), Acrylonitrile Butadiene Styrene (ABS), Polyethylene Terephthalate Glycol (PETG), Nylon or even Carbon Fiber reinforced plastic. Out of them, Nylon seems to be the most suitable due to its strength and low friction characteristics. Nylon is, for example, used in gears for all sorts of devices such as electric toothbrushes or microwaves. But nylon is also harder to print and requires an enclosure and proper ventilation due to toxic fumes. It is also more expensive than traditional PLA. As a result, it was decided to do the first prototype in PLA and only look at the possibility of using nylon if needed.

4.2 Exoskeleton Design

The design of the exoskeleton was done on a Computer-aided design (CAD) software called Fusion 360. A render of the design can be seen in figure 8. It consists of over 120 pieces that can be organized in nine distinctive groups: three plates and six extremity assemblies. One of those three plates is the Metacarpal plate and it is the center piece of

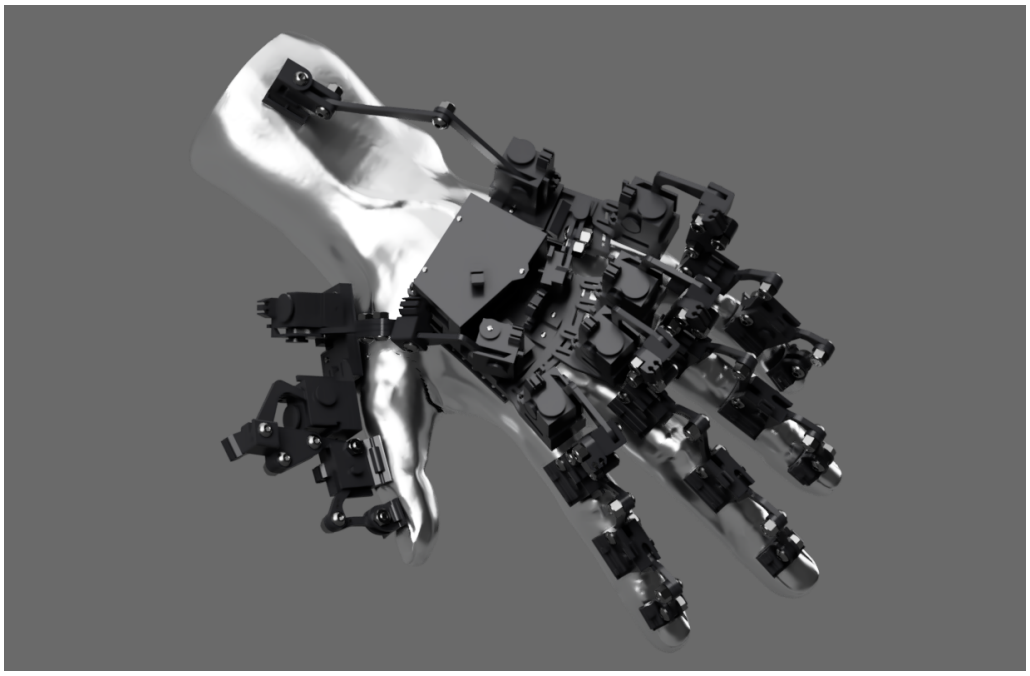

Figure 8: Render of the exoskeleton.

the exoskeleton. This plate houses the wire combiner PCBs and is the connection point for the two other plates as well as for three finger assemblies. The two other plates are the little finger plate and the thumb plate. The remaining finger assemblies as well as the wrist assembly are connected to those two plates. Certain important aspects of the

design will be looked at in more details in the following sub-chapters.

4.2.1 Hand Attachment Mechanism

One important design characteristics of the exoskeleton's design is the attachment mechanism. The human body has an organic shape which makes it hard to attach any parts to it. Some harness ideas were considered but it quickly became evident that using a glove is the simplest and probably best method. A compression glove was chosen as it is form fitting, yet strong enough to be sewed on. This shifted the problem to attaching the 3D printed pieces to the glove. Velcro was first tested but it wasn't stable enough by itself. Glue, while possible, would require a new glove every time a piece brakes and can therefore not be used. In the end, sewing was chosen for the plates situated on top of the hand (figure 9), elastic bands for the fingers (figure 10) and elastic bands combined with a hook-and-loop fastener system for the wrist.

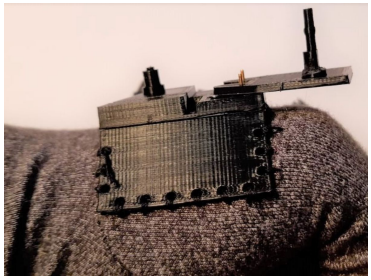

Figure 9: Attachment system: sewing.

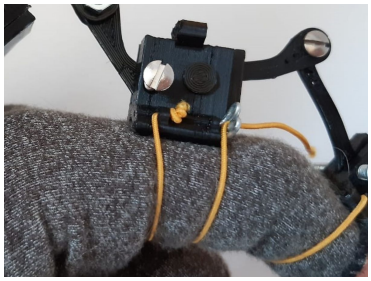

Figure 10: Attachment system: elastic bands.

Figure 11: Clay mold of the hand.

Of course sewing a flat and hard plastic piece onto an organic shape like the hand would not work too well. Consequently, ergonomic pieces were created to fit the hand more accurately. A clay model was used to form a mold. Figure 11 illustrates how the mold was sliced into smaller pieces. Several points across the surface, at equal distance from each other, were measured to form a 3D mesh. This mesh was then used to model the piece in Fusion 360. This process was then repeated for all the pieces coming into direct contact with the glove or the hand. This process also allows for a same exoskeleton design to be attached to the hands of various people by simply redesigning the mesh with a new mold.

4.2.2 Artificial Joints

According to the simplified model, described in chapter 2, there are two types of joints in the hand. The first type has one axis of rotation and is found on the fingers and between the metacarpal plate and the little finger plate. The other type of joint has two axes of rotation and is seen on the knuckles, the wrist and the thumb. Each type has its own artificial joint that moves synchronously with the actual joint, allowing it to be measured.

Figure 12 shows a finger assembly. On the left is the two axes artificial joint measuring the knuckle joint. It is comprised of nine pieces. There are some variations depending on where it is used but the main components remain identical. The mechanism allowing for the rotation around the vertical axis uses a snapping pin system. This pin fixes the ”up-down” movement of the assembly while allowing for the joint to rotate. The horizontal axis also uses a snapping pin. The potentiometers are placed on holders which get attached to the main piece. The purpose of the separation is to facilitate removing the potentiometers for the various situations that might require it. The pins are used to fix the potentiometers in place and to link the rotation of the joint to the potentiometer wiper. In the case of the knuckle joints the levers, connecting the joint to the next one, can rotate along their length. This is done to account for the curvature of the palm, described in chapter 2. The two middle artificial joints, seen in figure 12, are identical and measure one axis of

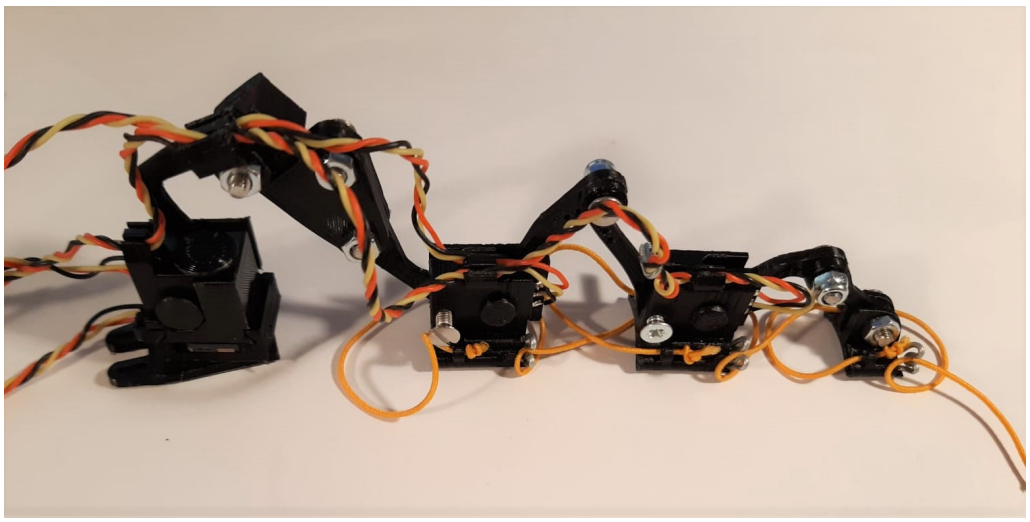

Figure 12: Finger assembly.

rotation. They are made of five distinct pieces. The narrow size of the finger does not allow for a snapping pin. As a consequence, the pin is fixed in place with a metal wire.

In order to reduce the friction of the pins and levers when rotating, silicon oil was used to lubricate them.

3D printing is an additive manufacturing process meaning that layers of plastic are printed on top of the previous layers. As a consequence it is impossible to print certain pieces, such as a bridge, without some sort of supporting structure. While these supporting structures allow for certain designs that would otherwise be impossible, they require a cleaning process that is time consuming. For this reason, with the exception of the ergonomic parts, the pieces of the entire exoskeleton were designed not to require such support.

4.2.3 Wire Management

The high number of sensors, with three wires each, requires a wire management method. Without it, the wires could cause excessive signal noise and mechanically hinder the natural movement of the hand. The wire combining PCB alleviates some of those problems for the wrist area but other methods are required for the wires going from the sensors to the previously mentioned PCB. One explored method was to use a common ground and power for all the sensors along one finger. The downside of this solution is that it would link four sensors to one another. This makes maintenance harder as it would require removing all four potentiometers to fix one. Due to this, a simpler method of designing attachment points for the wires was chosen. Three types of attachment systems were designed. The first one being a traditional clipping system. It can be seen in figure 12 on top of the artificial joints. The second system consists of various ”tunnels” through which the wires go. The difference between the clips and the ”tunnels” is that the latter are meant for multiple wires. The last system originated due to printing difficulties. Instead of clips, metal wires were used on the levers between the MP and PP.

4.3 Tolerances

Some parts of the exoskeleton design have really small details and push the 3D printer to its limit. As a consequence, the tolerances between different interacting parts are paramount to a successful print. The design of the hand exoskeleton requires four types of tolerances. The first type is a sliding tolerance. It can be found between the piece hold-

ing the potentiometer and the artificial joint into which it goes. This piece needs to slide in and out of the assembly but have enough friction so that it does not rotate with the levers. A test print ranging from 0.1 mm to 0.5 mm was designed. The result for the printer used in this thesis work, the Ender 3 pro, was a tolerance of 0.15 mm. Another type, found in the design, is a rotation tolerance. In this case the goal is to have two pieces rotate within each other with as little friction as possible but without sacrificing stability. These can be found on the knuckle joint or on the levers where screws are used. As for the previous tolerance type a test print was created resulting in 0.3mm as the best tolerance. Snap joints were also used in the knuckle joints. These joints are intended to snap together while still allow for rotation. They required extensive testing as multiple variables come into play to get a perfect fit. Finally, the exoskeleton is attached to the ergonomic plates with the help of screws. Instead of using an embedded bolt, the screw threads were created by the screws themselves through a simple process. The screws were heated up and pushed through a slightly smaller hole than the screw diameter.

These values were calculated for the specific printer used in this work. Even with the same printer model the tolerances might be different depending on a lot of factors. This variability is even more pronounced between different printer models. This makes reprinting this exoskeleton more challenging than anticipated as the tolerances for each piece needs to be updated for a new printer setup.

4.4 From Sensor Angle to Joint Angle

As described previously, the exoskeleton is mounted on the back of the hand. This configuration is chosen to ensure the best freedom of movement possible. The potentiometers, used to measure the angle of the joints, lay behind and above the actual joints. As a result, the angle measured by the sensor does not directly translate to the angle of the joint. A mathematical model was made to take this discrepancy into account. To transcribe the movement of all the joints of the hands three different types of artificial joint systems are required. The first one rotates around a horizontal axis. It transcribes all the hinge joints located on the fingers and between the 4th and 5th metacarpal bones. The second artificial joint also rotates around a horizontal axis but additionally contains a rotation around a vertical axis. It transcribes the movement of the knuckle joints and wrist joint. These two

artificial joints are described in more details in chapter 4.2.2. In the case of the knuckle joint the vertical axis of the artificial joint is designed the be precisely above the axis of rotation of the actual joint. Consequently, the angle of the potentiometer directly corresponds to the joint angle. The same mathematical model as with the hinge joints can be used for the horizontal axis. For the wrist the vertical rotation can be found through simple trigonometry while the horizontal axis again uses the hinge joint model. Finally, the third artificial joint system is used for the thumb. The same artificial joints as for the knuckles are used in this system. The position of these joints, relative to the actual thumb joints, makes the model transcribing the angles unique. The mathematical models for the hinge joints and thumb joint are derived in the next chapters.

4.4.1 Hinge Joint Model

A model of the finger joint can be seen in figure 13 which will be used by the following equations. The angle α is given by the potentiometer while the angle γ is the desired joint angle. The h and i segment represent the middle of the finger while the g and j segments represent the distance from the middle to the axis of rotation of the levers. As the dimensions of all the segments is known the position of the F and C point can be found out with simple trigonometry. Assuming that the point B is located at (0,0) the point C will simply be (h,0). The point F is accordingly given by equation (5).

$$F_{(x,y)} = (cos(\alpha) \cdot l, g + sin(\alpha) \cdot l) \tag{5}$$

With the coordinates of these points known, the strategy is to find the intersection points of the circles d and c. For the sake of readability the coordinates of the F and C point will be shown as (F_x, F_y) and (C_x, C_y). Accordingly, the equations describing the circles d and c are respectively given by equation (6) and (7), where r is given by the Pythagorean theorem $r = \sqrt{i^2 + j^2}$.

$$(x + F_x)^2 + (y - F_y)^2 = k^2 \tag{6}$$

$$(x + C_x)^2 + (y - C_y)^2 = r^2 \tag{7}$$

The x and y variables represent the coordinates of an arbitrary point along the circle. There are a few ways two circles can intersect with each other. Since it is known that one of the intersection points is the point E there are only two possibilities. The first being

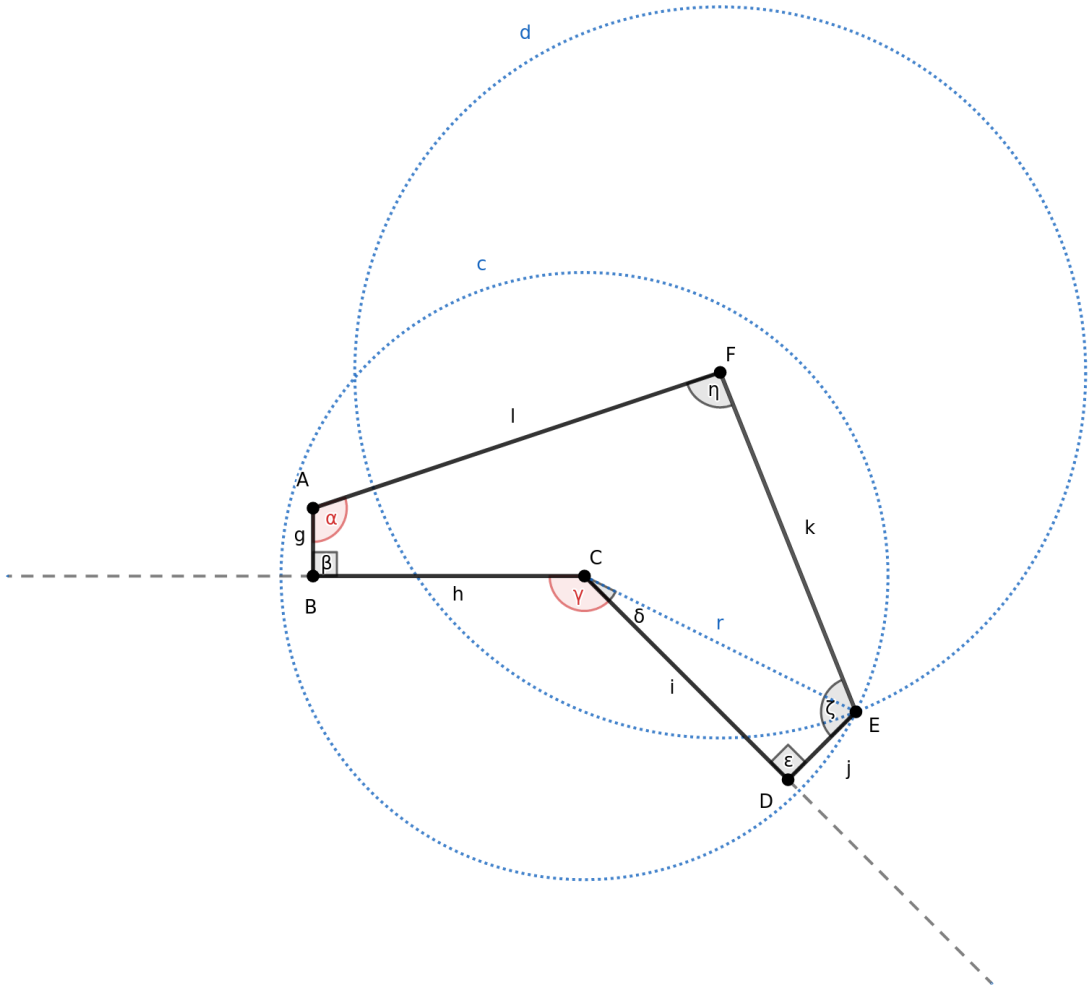

Figure 13: Mathematical Model of a Two Dimensional Joint

that the circles intersect only on point E while the other possibility is that there are two intersection points one being the point E. Having only one intersecting point requires for the segment k and r to be aligned. The way the joint is designed this is not possible as it it would either lead the k lever to go through the finger or have it going through the PLA parts. The conclusion is that the circles will intersect in two points. With that in mind, the two circle equations can be combined and solved for x and y. The intermediate steps of this derivation can be found in appendix 1. Combining equation (6) and equation (7) results in equation 8.

$$-2C_x x + 2F_x x - F_x^2 + C_x^2 + 2F_y y - 2C_y y - F_y^2 + C_y^2 = r^2 - k^2 \tag{8}$$

The next step is to solve for x with equation (9) and then substitute it back into one of the circle equations, in this case equation (6), resulting in the quadratic equation (10).

$$x = \frac{r^2 - k^2 + F_x^2 + F_y^2 - C_x^2 - C_y^2}{2 \cdot (F_x - C_x)} + \frac{C_y - F_y}{F_x - C_x} \cdot y \tag{9}$$

$$\begin{aligned}
&((\frac{C_y - F_y}{F_x - C_x})^2 + 1) \cdot y^2 + 2 \cdot ((\frac{r^2 - k^2 + F_x^2 + F_y^2 - C_x^2 - C_y^2}{2 \cdot (F_x - C_x)}) \cdot (\frac{C_y - F_y}{F_x - C_x}) - \\
&F_x \cdot (\frac{C_y - F_y}{F_x - C_x}) - F_y) \cdot y + (\frac{r^2 - k^2 + F_x^2 + F_y^2 - C_x^2 - C_y^2}{2 \cdot (F_x - C_x)})^2 \\
&- 2 \cdot F_x \cdot (\frac{r^2 - k^2 + F_x^2 + F_y^2 - C_x^2 - C_y^2}{2 \cdot (F_x - C_x)}) + F_x^2 + F_y^2 - k^2 = 0
\end{aligned} \tag{10}$$

Once in the quadratic form the famous quadratic formula, equation (11), can be used to extract A, B and C, given by equation (12). This is done to maintain a certain level of readability.

$$\frac{-B \pm \sqrt{B^2 - 4 \cdot A \cdot C}}{2 \cdot A} = 0 \tag{11}$$

$$\begin{aligned}
A =& (\frac{C_y - F_y}{F_x - C_x})^2 + 1 \\
B =& 2 \cdot ((\frac{r^2 - k^2 + F_x^2 + F_y^2 - C_x^2 - C_y^2}{2 \cdot (F_x - C_x)}) \cdot (\frac{C_y - F_y}{F_x - C_x}) - F_x \cdot (\frac{C_y - F_y}{F_x - C_x}) - F_y) \\
C =& (\frac{r^2 - k^2 + F_x^2 + F_y^2 - C_x^2 - C_y^2}{2 \cdot (F_x - C_x)})^2 \\
& - 2 \cdot F_x \cdot (\frac{r^2 - k^2 + F_x^2 + F_y^2 - C_x^2 - C_y^2}{2 \cdot (F_x - C_x)}) + F_x^2 + F_y^2 - k^2
\end{aligned} \tag{12}$$

Solving this quadratic equation gives two answers for y denoted y_1 and y_2 (eq. 13). These results are then substituted back in the original circle equation (6) giving the two x coordinates for the intersection points in equation (14).

$$y_{1,2} = \frac{-B \pm \sqrt{B^2 - 4 \cdot A \cdot C}}{2 \cdot A} \tag{13}$$

$$x_1 = \frac{r^2 - k^2 + F_x^2 + F_y^2 - C_x^2 - C_y^2}{2 \cdot (F_x - C_x)} + \frac{C_y - F_y}{F_x - C_x} \cdot \frac{-B + \sqrt{B^2 - 4 \cdot A \cdot C}}{2 \cdot A}$$
$$x_2 = \frac{r^2 - k^2 + F_x^2 + F_y^2 - C_x^2 - C_y^2}{2 \cdot (F_x - C_x)} + \frac{C_y - F_y}{F_x - C_x} \cdot \frac{-B - \sqrt{B^2 - 4 \cdot A \cdot C}}{2 \cdot A} \quad (14)$$

Having found the two intersection points a choice needs to be taken as to which point is the correct one. The rotation of lever l is limited as the finger prevents the point F from going below the point C in either direction. This has as consequence that the x coordinate of the E point will always be bigger than that of the second intersection point. Having the coordinates of the point E makes it possible to calculate the angle representing $\gamma + \delta$ according to equation (15).

$$\gamma + \delta = 180° + \text{arcsin}(\frac{E_y}{r}) \quad (15)$$

As we know the angle δ, given by equation (16), we can finally calculate the angle of the joint γ with equation (17).

$$\delta = \text{arctan}(\frac{j}{i}) \quad (16)$$

$$\gamma = 180° + \text{arcsin}(\frac{E_y}{r}) - \text{arctan}(\frac{j}{i}) \quad (17)$$

4.4.2 Thumb Model

The thumb, as described in the anatomical chapter, is a slightly more complex joint due to its saddle joint and the 45° attachment point. What makes the model particularly difficult is the position of the sensors. Unlike with the finger joints, the potentiometers cannot be easily aligned with the axis of rotation. This means that an alternative placement was chosen with one side attached to the metacarpal plate and the other to the thumb plate. Figure 14 models this setup, looking at the hand from a profile perspective. This allows the vertical position of the thumb to be defined using the angle α. The Point B represents the saddle joint and Point A the top of the hand directly above it. The potentiometers are located on point E, F and C. The distances of segments l, m, o and r are known as well

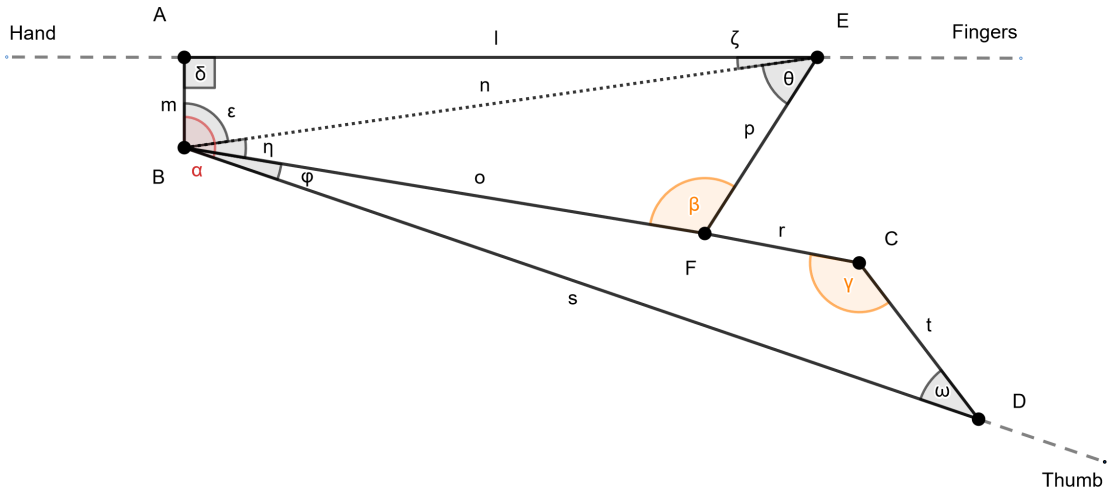

Figure 14: Thumb model with a side perspective.

as the angles δ, β and γ. With this knowledge, the strategy to find the angle α is simply trigonometry and the sin law. Knowing m and l allows p to be calculated according to equation 18.

$$n = \sqrt{m^2 + l^2} \tag{18}$$

The sine law, equation (19), allows for the angles ϵ (eq. 20), η (eq. 21) and ϕ (eq. 22) to be calculated.

$$\frac{a}{\sin(\alpha)} = \frac{b}{\sin(\beta)} = \frac{c}{\sin(\gamma)} \tag{19}$$

$$\begin{aligned} \frac{n}{\sin(\delta)} &= \frac{l}{\sin(\epsilon)} \\ \sin(\epsilon) &= \frac{l}{n} \cdot \sin(\delta) \\ \epsilon &= \arcsin\left(\frac{l}{n} \cdot \sin(\delta)\right) \end{aligned} \tag{20}$$

$$\begin{aligned} \frac{n}{\sin(\beta)} &= \frac{o}{\sin(\theta)} \\ \theta &= \arcsin\left(\frac{o}{n} \cdot \sin\beta\right) \\ \eta &= 180 - \beta - \arcsin\left(\frac{o}{n} \cdot \sin(\beta)\right) \end{aligned} \tag{21}$$

$$\frac{s}{\sin(\gamma)} = \frac{t}{\sin(\phi)}$$
$$\phi = \arcsin\left(\frac{t}{s} \cdot \sin(\gamma)\right) \tag{22}$$

With these angles calculated, it is possible to calculate α with the help of equation (23).

$$\alpha = \arcsin\left(\frac{l}{n} \cdot \sin\delta\right) + (180 - \beta - \arcsin\left(\frac{o}{n} \cdot \sin(\beta)\right)) + \arcsin\left(\frac{t}{s} \cdot \sin\gamma\right) \tag{23}$$

The angle alpha represents the abduction and adduction movement of the thumb described in chapter 2.2.

In order to define the angle of the extension and flexion movement, an additional model is required. Figure 15 shows the thumb from the back, looking towards the fingers. The

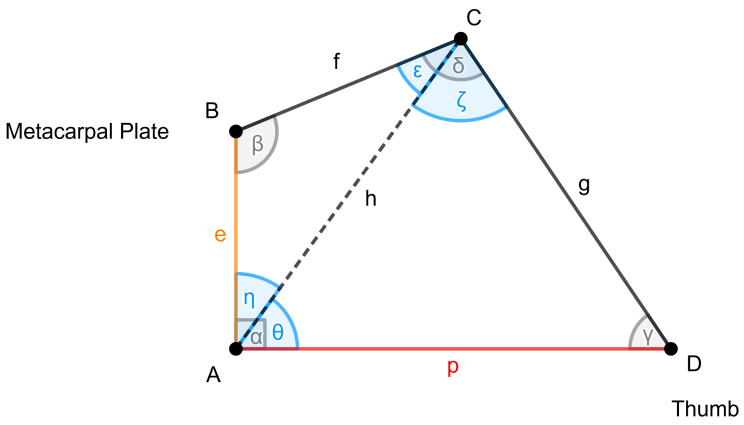

Figure 15: Thumb model with a back perspective

segment e is the vertical distance separating the top of the hand and the thumb. It can be calculated with the help of the angle α, from equation (23), and simple trigonometry. The calculation can be seen in equation (24). The variables of that equation come from figure 13.

$$e = m + \tan\left((\epsilon + \eta) - 90\right) \cdot o \tag{24}$$

The segments f and g represent the levers between the thumb plate and the metacarpal plate. The angle β is given by a potentiometer. With these variables known, it is possible

to use the law of cosines (eq. 25) to calculate h as can be seen in equation (26).

$$c = \sqrt{a^2 + b^2 - 2 \cdot a \cdot b \cdot \cos y} \tag{25}$$

$$h = \sqrt{e^2 + f^2 - 2 \cdot e \cdot f \cdot \cos \beta} \tag{26}$$

With the segment h known, the sin law (eq. 19) can be used to calculate the angle η with equation (27).

$$\eta = \arcsin\left(\frac{f}{h} \cdot \sin \beta\right) \tag{27}$$

The angle α, from figure 15, is a right angle. Consequently, the angle θ can be calculated with equation (28).

$$\theta = 90 - \arcsin\left(\frac{f}{h} \cdot \sin \beta\right) \tag{28}$$

The sin law gives us the angle γ (eq. 29). Knowing the angle θ and γ allows us to find the angle ζ (eq. 30). With the help of the sin law, it is now possible to find the length of segment p, given by equation (31).

$$\gamma = \arcsin\left(\frac{h}{g} \cdot \sin \theta\right) \tag{29}$$

$$\zeta = 180 - \theta - \gamma \tag{30}$$

$$p = \gamma \cdot \frac{\sin \zeta}{\sin \gamma} \tag{31}$$

The segment p, from figure 15, represents the distance between the potentiomter on the metacarpal plate and the potentiomter on the thumb plate. In order to find the angle representing the extension and flexion movements, the law of cosines can be used. Figure 16 models this situation, looking at the hand from the top. Equation (32) is used to solve for the angle β.

$$\beta = \arcsin\left(\frac{f^2 + h^2 - p^2}{2 \cdot f \cdot h}\right) \tag{32}$$

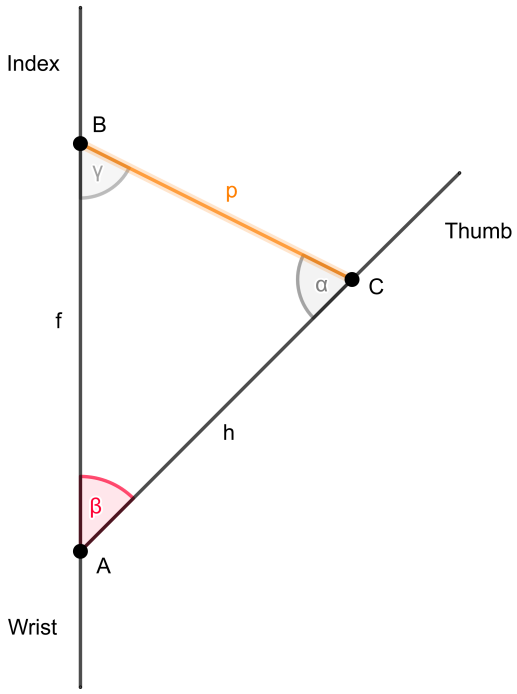

Figure 16: Thumb model Left Rigth From the Top

The models, used to calculate the angles α (eq. 23) and β (eq. 32), contain inaccuracies. The thumb metacarpal bone is surrounded by a muscle. This muscle contracts while moving the thumb. As a consequence, the angles measured by the potentiomters are not only influenced by the movement of the bone but also by the contraction of the muscle. Without this effect the angle ϕ, in figure 14, would be 0°. The potentiomter, located on point C of the same figure, is used to reduce the loss of accuracy induced by this issue.

5 Platform Performance

The performance of this position and movement acquisition system is evaluated in relation to the goals described in the introduction. To fulfill the purpose of gathering real-time hand position data to train the neural network of a gesture recognizing wristband four performance criteria were defined. The first goal was to transcribe the position and movements of the hand with high anatomical fidelity. The second objective was to have an uncertainty in the angle measurements with a standard deviation of 0.15. Thirdly, the exoskeleton needed to be fast to setup and comfortable to wear for longer periods of time. Finally, the device required affordability while remaining easy to build and maintain. These four performance criteria will be analyzed below.

5.1 Anatomical Fidelity

As described in chapter 2 certain movements and anatomical properties of the hand were disregarded from the outset of the design. These included for example a simplified wrist motion and a disregard for the finger's medial rotations. Other restrictions come from the design of the exoskeleton. The full extension of the fingers and thumb is not possible due to the potentiometers holders on the PP and the knuckle touching each other. Some movements, such as moving one finger over the other are also restricted due to the exoskeleton. Finally, while possible a fist with the thumb on the inside is also slightly restricted. Apart from the restrictions just mentioned, the exoskeleton performs as intended.

5.2 Accuracy and Precision

Before going any further, it is important to clarify the difference between accuracy and precision. These terms are often used interchangeably in colloquial language and therefore can lead to confusion. Accuracy refers to the distance between the average measured value and the true value. The more accurate the measurements are, the smaller this distance is. Precision, on the other hand, refers to how spread out the measurements are.

The more spread out they are, the less precise they are. Together these two concepts describe the uncertainty of a value. To provide a more intuitive understanding a depiction of this concept can be found in figure 17.

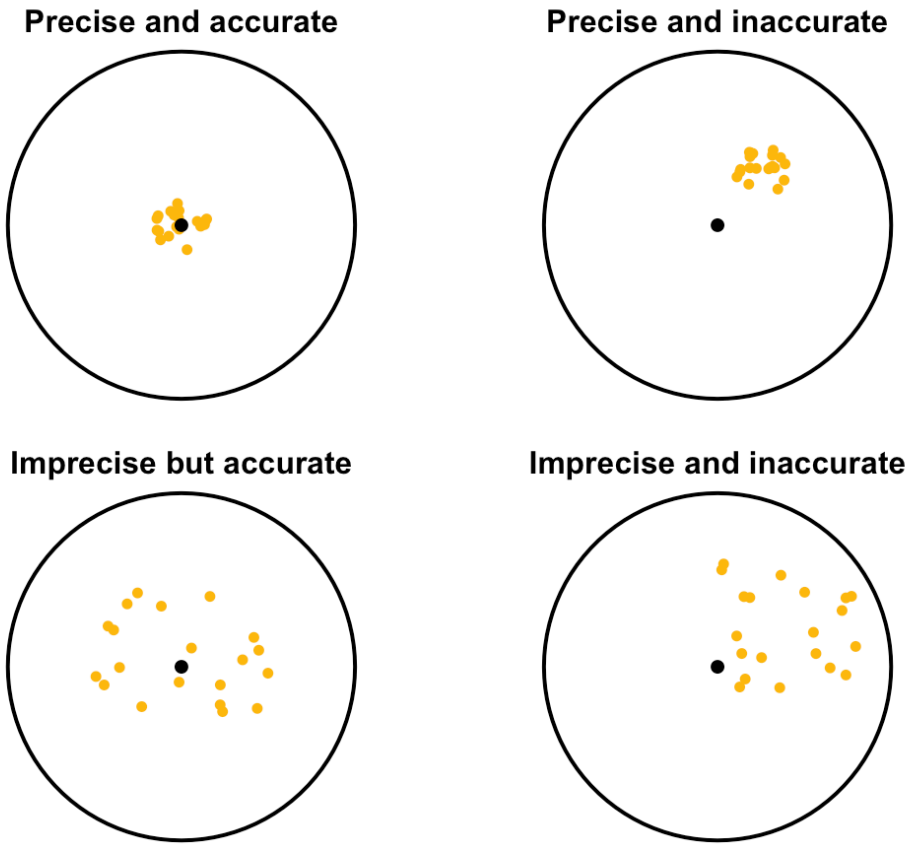

Figure 17: Accuracy and Precision, copied from Dunn (2021) [14, section 5.2]

As detailed in the chapter 3.1, the sensors used in this project are the sv03a103 potentiometers from Murata. The datasheet, provided by the manufacturer, gives information on their precision and accuracy [12]. Unfortunately, these numbers do not take into account the effects of the environment in which the sensors are used. The electronic circuit connecting all the potentiometers to the Arduino will affect the precision and accuracy. The connecting points between the sensors and the measured joint angles will do so as well. On top of that, the models transcribing the sensor angles to the joint angles (described in chapter 4.4) will also add some uncertainty to the system as they rely on unreliable hand measurements. To take these three aspects into account, the precision and accuracy of the sensors need to be calculated for this specific use case. Before doing so, some steps can be taken to improve the precision of the accuracy of the sensors themselves. The precision can be increased by taking a higher number of measurements per sample while

calibration can help with the accuracy.

The precision of a measurement is defined by a probability density function. It describes how successive measurements, acquired identically, are spread out around the mean value of the sample formed by those measurements. Different density functions can require different analytical tools, it is therefore important to know which one describes this situation the best. Figure 18 shows an estimate of the probability distribution. A potentiometer was connected to the circuitry and 10'000 samples were taken with the sensor in a static position. The mean of the samples was subtracted from the samples in order to center the graph. A Kernel Density Estimation (KDE) with a Gaussian kernel and a bandwidth of 0.5 was used to plot the samples.

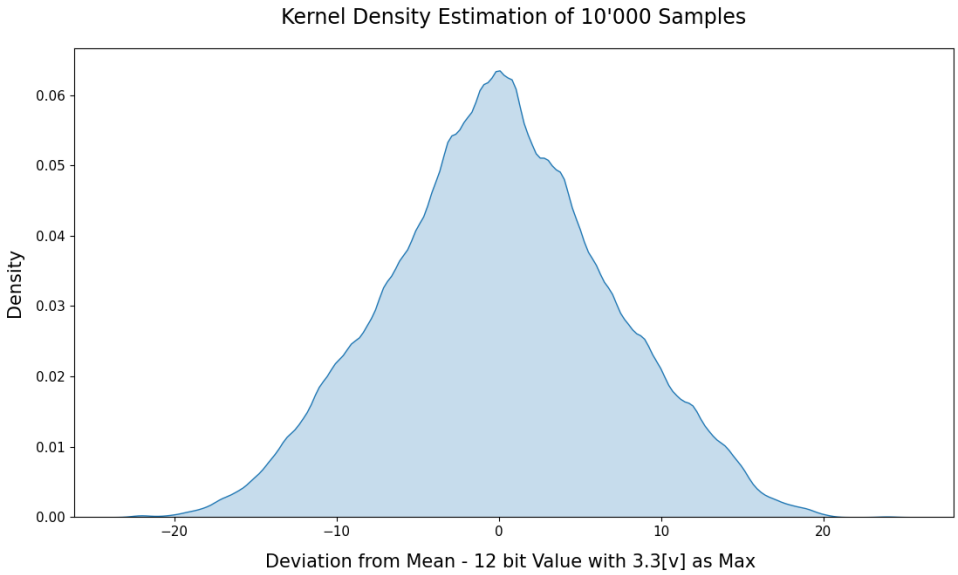

Figure 18: Distribution function estimate with the help of a KDE

As can be seen from the graph, the distribution has the characteristic properties of a normal distribution. It is symmetric around the mean and follows the well-known bell shape. A normal distribution is defined by its mean and a standard deviation. There are two distinct standard deviations, the sample standard deviation and the population standard deviation. In this situation the sample standard deviation is used as the measurements represent a sample of a bigger population. Increasing the number of samples per measurement improves the precision but it also increases the time per measurement. The original goal was to have a 60 Hz update rate. To take this factor into account, when choosing the ideal number of samples per measurement, a specific procedure was followed to measure the precision. The complete circuit was assembled and connected with

the potentiometers in a static position. Including the final circuit allowed to get an accurate estimate of the time required per measurement. For each potentiometer 10’000 samples were taken. As the precision can vary within the measuring range of a sensor, the measurements were also taken at three different angles (90°, 180°, 270°) for each sensor. The mean of the samples was then subtracted from each measurement. This was done so that visual comparison of the probability distribution between different potentiometers is easier. Otherwise the differences between the set angles would shift the mean up and down from one potentiometer to the next.

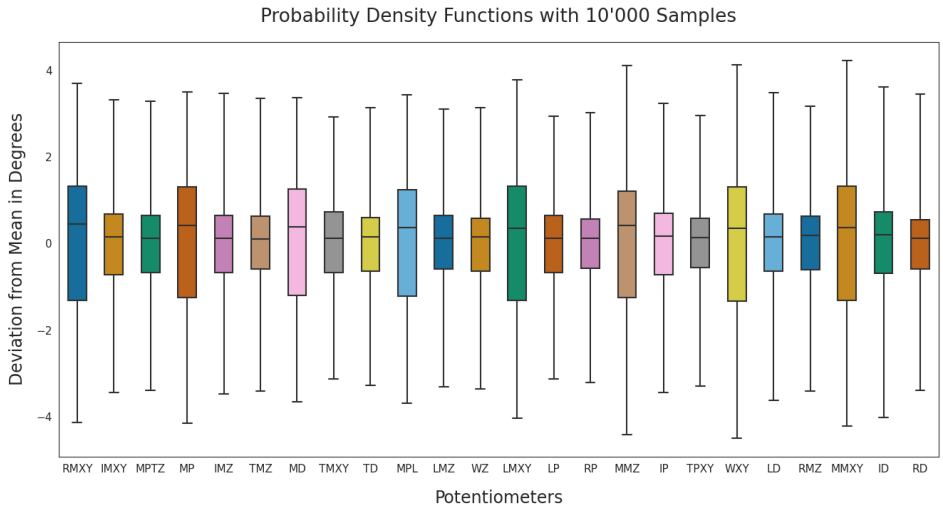

Figure 19: Probability density function of each potentiometer represented through a box-and-whisker plot.

The results can be seen in figure 19. The potentiometers are named following a simple naming convention. The first letter defines the finger, the second letter corresponds to a certain bone of that finger and the last letters represent the axis in case of the knuckle joints. The potentiometers housed on the plates have their first letters after the plates themselves. The probability density function of each potentiometer was plotted using a Whisker and Box plot. As can be seen from the graph, such a plot consists of three parts. The whiskers, which are the T-shaped ends, represent in this case the 1st and 99th percentile. Meaning that one percent of the measurements lies below and one percent above the whiskers. The second part is the colorful box, whose edges represent the first and second quartile. In other words: the 25th and the 75th percentile. Finally, the line within the box is the median. It is important to keep in mind that the percentiles represented do not correspond directly to the sample standard deviation. The empirical rule (also known as the Three Sigma Rule) states that 68% of the measurements will fall within

one standard deviation, 95% within two and 99.7% within three standard deviations [15, 553]. But the interval between the whiskers represents 98% of the samples and the box represents 50%. Another reason is that the empirical rule is actually an approximation and it only stands for a normal distribution while a real life system is rarely perfectly normally distributed. The percentiles also only describe the given samples and do not take into account errors due to a possibly small sample size. However, these last two factors are negligible since a high sample size is used and the distribution is close from being an ideal normal distribution.

Going back to figure 19 two observations can be made. The first being that every third potentiometer has a worse precision. This can be seen when looking at the size of the boxes. The bigger the box the lower the precision. The way the signals are routed through the multiplexers suggests some damage or bad connection with the first multiplexer. The second information this graph provides is that the result is really far from the starting goal which was a standard deviation of 0.15. 98% of the samples fluctuate between roughly -3.5° and 3.5°, leaving out the malfunctioning multiplexer the average sample standard deviation of the potentiometers at 180 degrees is 1.2. As the mean and the population (sample count) is the same for each potentiometer, the standard deviation can simply be averaged. Otherwise these factors would need to be taken into account when calculating the combined standard deviation value. At 90 degrees the average sample standard deviation is 1.2 and 1.3 at 270 degrees. The precision therefore seems to be negligibly affected by the position of the sensor along its range.

As mentioned above, the downside of averaging successive samples to increase precision is a longer acquisition time required per measurement. The goal was to take 60 measurements per second therefore there is an upper limit to how many successive readings can be taken for one measurement. Table 1 demonstrates that 100 samples would be required to satisfy the original goal of a standard deviation of 0.15. But as can be seen, this would drop the measurements per second to only 8. While analyzing ways to increase the measurement speed it became apparent that the function AnalogRead(), of the Arduino Nano 33 BLE, operating the ADC is the bottleneck. It was measured that the function takes roughly $115\mu s$ to complete one reading. With 24 potentiometers and 100 samples per measurements equates to $24 * 100 * 100[\mu s] = 240'000[\mu s]$ or 0.24s while in order to respect a 60 Hz measurement rate, one measurement can only take

Table 1: Sample Count

Samples per Measurement	Standard Deviation in Degree	Sample Percent within one Degree	Measurements per Second
1	1.21	40%	364
5	0.59	64%	136
13	0.38	82%	60
25	0.27	93%	33
50	0.19	98%	17
100	0.15	99%	8

$1/60 = 0.016[s]$. This could be solved by using a custom function with less overhead to use the ADC. The nrf52840 chip used on the Arduino is theoretically capable of reducing the acquisition time to $5\mu s$ [16, 378]. This would increase the sampling rate enough but it is not clear if it would work as increasing the sampling rate of the ADC also increases the noise. Staying with the basic function provided by the Arduino library, 13 readings per sample was chosen as it is the highest reading count that still respects the 60 Hz sampling rate. With this, the final standard deviation is 0.4. To get a more intuitive understanding of the final precision it was numerically calculated from the dataset how many samples lie within -0.45 and 0.45 for a given sample count. With the chosen 13 samples, this equates to 82% while definitely not as good as the 99.7% of a 0.15 standard deviation, it is still quite good.

Precision is only one part of the uncertainty. Simply taking the value above of 0.4 would assume that there is no bias. In other words, that the accuracy is perfect. In the context of this thesis work, measuring the accuracy is much harder than the precision. In order to measure the accuracy of the sensors, it is necessary to determine the true angle without the sensors. This true angle can then be used as a standard against which the values from the sensors can be compared. The distribution of the variation between the two angles gives the accuracy distribution. One way of finding this real angle is to manually measure the angle with a protractor. The question then becomes how precise this manual measurement is. In order to answer that question, a manual measurement of the same angle was done 25 times with 200 samples per measurement. Taking the mean of the 200 samples reduces the precision errors of the potentiometer itself. The standard error describes how close to the true value the mean will be. In the formula for the standard

error, equation (33), the letter sigma(σ) stands for the population standard deviation.

$$\sigma_{\bar{x}} = \frac{\sigma}{\sqrt{n}} \tag{33}$$

As only the sample standard deviation is known, the standard error will be an approximation. With 200 samples the standard error is $\frac{0.38}{\sqrt{200}} \approx 0.0000095$, which is well below the resolution of the sensor. Therefore, it can be assumed that the mean value is the true value. The resulting standard deviation of the 25 mean values was 0.3. This signifies that, when manually repeating the measurement multiple times, 99.7% of the measurements will fall between -0.9°and 0.9°of the real angle.

With an estimate of the true value found, the accuracy can be measured by comparing it to the value gotten from the sensors. The values were compared and plotted, in figure 20, for four potentiometers at a 5° interval and for 3 potentiometers at a 10° interval. As demonstrated above, the precision of the sensor was fixed by taking the mean of multiple samples. More samples should have been taken for each angle and potentiometer combination to account for the errors in the manual measurement of the true angle. Unfortunately, the time required to do so would be prohibitive with the measurement system used. The graph, in figure 20, shows a linear correlation between the deviation from the true value and the measured angle. This is where the calibration comes in handy. A least squared fitted line ($y = 0.007 \cdot x - 17.92$) was calculated from the dataset. Subtracting the y of this line from the sensor value will have the effect of removing the linear correlation. The standard deviation after the calibration is 3.17. This high number suggests that an individual calibration for each sensor would be required as the manual measurement errors are not big enough to explain this spread.

With the accuracy and the precision improvements made, the actual uncertainty of the final device can be measured. The exoskeleton is composed of three different joint types described in chapter 4.4.

In order to test the joints an artificial joint was created, see figure 22. It simulates to range of motion of those joints and measures the actual position thanks to potentiometers. On top of it are attached the potentiometer holders. The difference between the angles given by the sensors on the joint versus the sensors in the holders will give the accuracy and precision of the device. Figure 21 illustrates the result for the first joint type. The standard

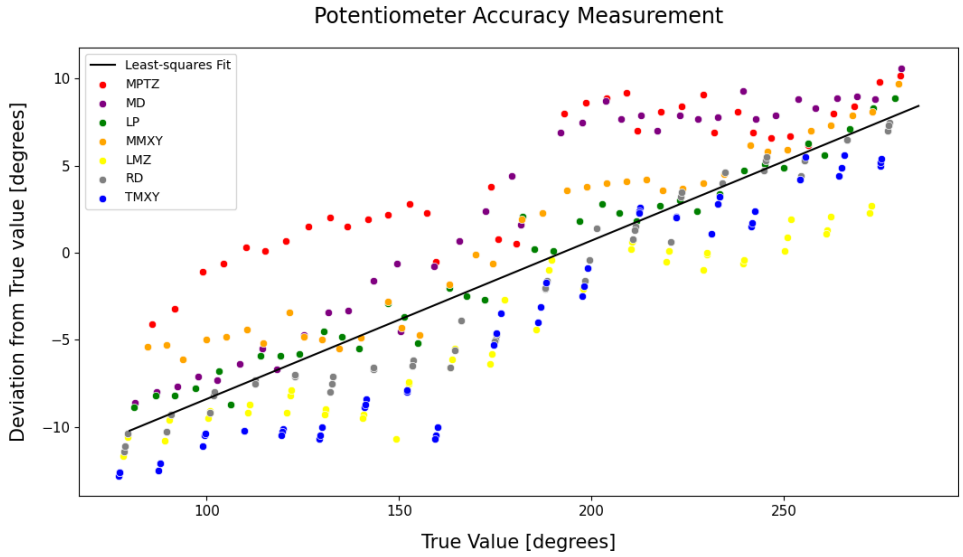

Figure 20: Potentiometer Accuracy Measurement.

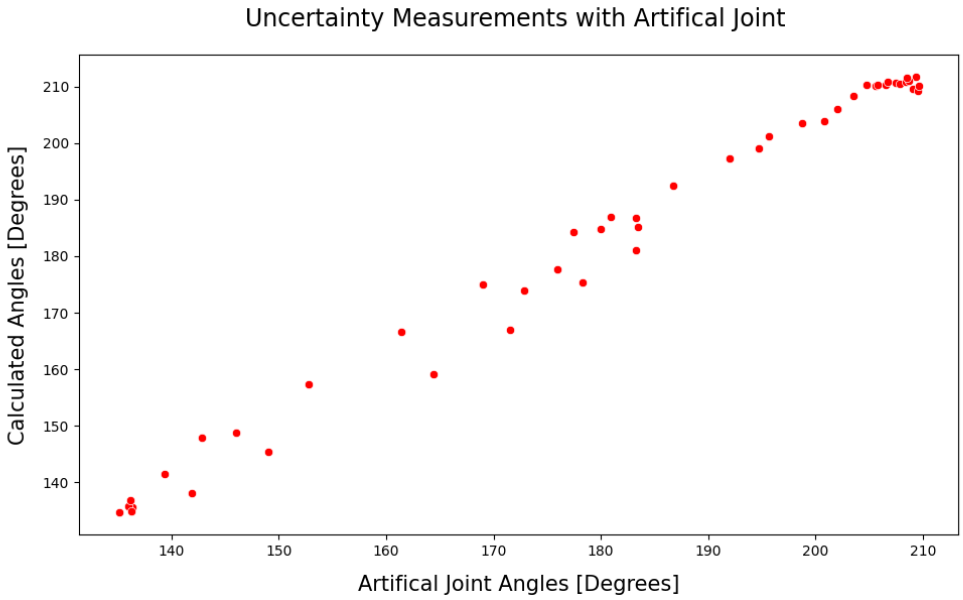

Figure 21: Artificial Joint Measurement.

deviation in this case is 3.09. The value being the same as when testing the accuracy of the sensors themselves suggests that the effects of the connecting points are negligible compared to the errors introduced by the lack of individual calibration of the sensors. The same result is found when looking at the accuracy of the thumb joint. In conclusion, the original goal of an uncertainty with a 0.15 standard deviation was not achieved. The cause for the higher uncertainty is due to the relatively poor accuracy of the sensors. Other effects cannot be distinguished in the final setup without better individual calibration of the sensors. Due to the sufficiently high precision of the potentiometers, the calibration would

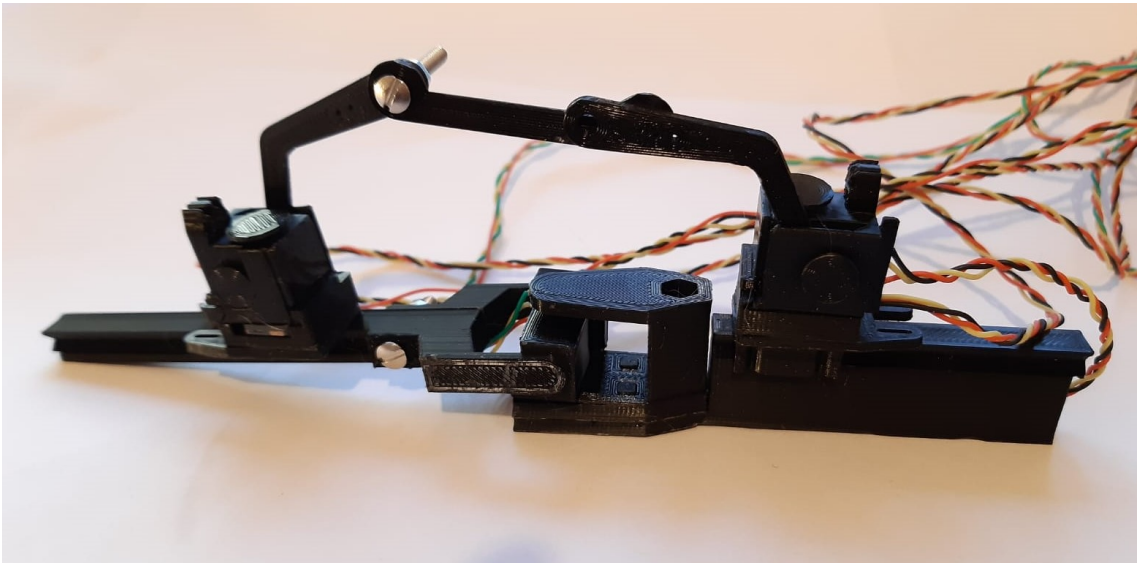

Figure 22: Artificial Joint Measurement.

be possible with a more time-efficient and reliable process.

5.3 User-friendliness

The first factor that was looked at, is how quickly the device can be set up and ready to use. The glove, as expected, is really easy to put on. On the other hand, each finger requires multiple elastic bands to be put on and adjusted. This takes a considerable amount of time and makes the setup quite tedious. In addition to this, multiple manual measurements need to be taken in order to properly calculate the joint angles. This long setup time is, on the other hand, compensated by the possibility to wear the glove for an extensive time. This is made possible by the adjustable elastic bands. The other tested attachment methods resulted in a constrained blood flow that would severely limit the wearing time. This can still happen with the chosen system but as the elastic bands can easily be tuned while wearing the glove it does not require to stop recording data.

5.4 Building Process, Maintenance and Affordability

Building the exoskeleton, while relatively easy, is quite time-intensive. This is mostly due to the printing time which requires a few days without using multiple printers. Some other time intensive aspects are sewing and soldering but they can be done within one day. The

construction itself is quite robust and does not suffer from any major problems. Two weak points of the design were detected during the final testing phase. The first weakness are the threads made by inserting a hot screw into the piece. These threads become loose after the pieces have been screwed and unscrewed multiple times. The second problem comes from some of the pins breaking accidentally. These pieces can, of course, be reprinted but this results in undesired maintenance. The final device has cost roughly 180 euros to develop. It is important to keep in mind that this price can fluctuate a lot. The price of components can be higher or lower depending on the amount that is being ordered and shipment costs. Certain components such as screws or solder might already be available or will not be fully utilized. Taking these factors into account it is possible to give a range from around 100 euros to 200 euros for the final device cost. This range does not include the price for a 3D printer. While quite a large price range, it gives an idea of the order of magnitude. Similar devices that are commercially available can cost from around 600 euros (VRFREE by sensoryx) to a few thousand euros (Manus™Prime 2) at the time of writing this thesis. In this context, the resulting price range achieved is quite affordable.

6 Conclusions

The goal of this project was to acquire the position and movements of the hand in real time in order train a neural network. To this end, an exoskeleton, using potentiometers, was designed. While the design is usable, it does not satisfy the original goals in accuracy and precision, which was a standard deviation of 0.15 degrees. However, the reason for the uncertainty suggests that the desired accuracy and precision can be achieved by simple improvements without a ground up redesign. Individual sensor calibration can solve the accuracy issue and the use of an external ADC or a custom arduino AnalogRead() function can solve the relative lack of precision. On the mechanical side, the exoskeleton fulfils its goal. First, it is affordable, as it is cheaper than a lot of the alternative options and secondly, it is easy to use and build. Some possible improvements include a system to adapt the 3D model's tolerances to a printer setup. This would make the building process feasible even without 3D printing and 3D modeling experience. Other aspects such as the fragile pins or the plastic threads could also be improved upon to reduce the need for maintenance. In conclusion, some additional work would be required to use the system for its intended purpose but this work has shown that it is a viable option to gather real-time hand position data with ease and at a low entry price.

Bibliography

1 McIntosh J, McNeill C, Fraser M, Kerber F, Löchtefeld M, Krüger A. EMPress: Practical Hand Gesture Classification with Wrist-Mounted EMG and Pressure Sensing. 2016;p. 2332–2342. Available from: https://doi.org/10.1145/2858036.2858093.

2 Iglovikov V, Rakhlin A, Kalinin A, Shvets A. Pediatric Bone Age Assessment Using Deep Convolutional Neural Networks. 2017;.

3 Hirt B, Seyhan H, Wagner M, Zumhasch R. Hand and Wrist Anatomy and Biomechanics - A Comprehensive Guide. Thieme; 2017.

4 AE F. Our thumbs. 2002;Available from: https://www.tandfonline.com/doi/abs/10.1080/08998280.2002.11927870.

5 Rahman A, Al-Jumaily A. Design and Development of a Bilateral Therapeutic Hand Device for Stroke Rehabilitation. International Journal of Advanced Robotic Systems. 2013 12;10:1.

6 'Sensor', Dictionary. Merriam-Webster.com; 2021 [cited April 24, 2021]. Available from: https://www.merriam-webster.com/dictionary/sensor.

7 Fraden J. Handbook of Modern Sensors. Physics, Designs, and Applications, Fifth Edition . Springler; 2016.

8 Das A, Tashev I, Mohammed S. Ultrasound based gesture recognition. 2017 IEEE International Conference on Acoustics, Speech and Signal Processing (ICASSP). 2017;p. 406–410.

9 Salchow-Hömmen C, Callies L, Laidig D, Valtin M, Schauer T, Seel T. A Tangible Solution for Hand Motion Tracking in Clinical Applications. Sensors. 2019;19. Available from: https://www.mdpi.com/1424-8220/19/1/208.

10 Doosti B. Hand Pose Estimation: A Survey. CoRR. 2019;abs/1903.01013. Available from: http://arxiv.org/abs/1903.01013.

11 Aqsa, Ali and Aleem, Mushtaq and Attaullah, Memon and Monna. Hand Gesture Interpretation Using Sensing Glove Integrated with Machine Learning Algorithms. Vol:10, No:11, 2016;.

12 Rotary Position Sensors; 2017. R51E. Available from: https://www.murata.com/~/media/webrenewal/support/library/catalog/products/sensor/rotaryposition/r51e.ashx.

13 Hoad TF. The Concise Oxford Dictionary of English Etymology. Oxford University Press; 2002.

14 Dunn, Peter K . Scientific Research Methods: An introduction to quantitative research in science and health.; 2021. Available from: https://bookdown.org/pkaldunn/Book.

15 Grafarend EW. Linear and Non linear Models: Fixed Effects, Random Effects, and Mixed Models. Walter de Gruyter; 2006.

16 nRF52840; 2019. Available from: https://content.arduino.cc/assets/Nano_BLE_MCU-nRF52840_PS_v1.1.pdf.

1 Angle Formula Derivation

This annex contains the step-wise derivations of the potentiometer angle to joint angle formulas.

1.1 Intersection Points Between two Circles

Equations of circle c and d:

$$(x + F_x)^2 + (y - F_y)^2 = k^2 \qquad \text{(d circle)}$$
$$(x + C_x)^2 + (y - C_y)^2 = r^2 \qquad \text{(c circle)}$$

Expand:

$$x^2 - 2F_x x + F_x^2 + y^2 - 2F_y y + F_y^2 = k^2 \qquad \cdot(-1)$$
$$x^2 - 2C_x x + C_x^2 + y^2 - 2C_y y + C_y^2 = r^2$$

Combine:

$$-2C_x x + 2F_x x - F_x^2 + C_x^2 + 2F_y y - 2C_y y - F_y^2 + C_y^2 = r^2 - k^2$$

Isolate x:

$$(-2C_x + 2F_x) \cdot x = r^2 - k^2 - C_y^2 + F_y^2 + 2C_y y - 2F_y y - C_x^2 + F_x^2 \qquad \div(-2C_x + 2F_x)$$
$$x = \frac{r^2 - k^2 - C_y^2 + F_y^2 - C_x^2 + F_x^2 + (2C_y - 2F_y) \cdot y}{-2C_x + 2F_x}$$

Simplify:

$$x = \frac{r^2 - k^2 + F_x^2 + F_y^2 - C_x^2 - C_y^2}{2 \cdot (F_x - C_x)} + \frac{C_y - F_y}{F_x - C_x} \cdot y$$

Substitute x in the expanded d circle equation:

$$(\frac{r^2-k^2+F_x^2+F_y^2-C_x^2-C_y^2}{2\cdot(F_x-C_x)}+\frac{C_y-F_y}{F_x-C_x}\cdot y)^2-$$
$$2F_x\cdot(\frac{r^2-k^2+F_x^2+F_y^2-C_x^2-C_y^2}{2\cdot(F_x-C_x)}+\frac{C_y-F_y}{F_x-C_x}\cdot y)+F_x^2+y^2-2F_yy+F_y^2=k^2$$

Expand:

$$(\frac{r^2-k^2+F_x^2+F_y^2-C_x^2-C_y^2}{2\cdot(F_x-C_x)})^2+2\cdot(\frac{r^2-k^2+F_x^2+F_y^2-C_x^2-C_y^2}{2\cdot(F_x-C_x)})\cdot(\frac{C_y-F_y}{F_x-C_x})\cdot y+$$
$$(\frac{C_y-F_y}{F_x-C_x})^2\cdot y^2-2F_x\cdot(\frac{r^2-k^2+F_x^2+F_y^2-C_x^2-C_y^2}{2\cdot(F_x-C_x)})+$$
$$2F_x\cdot\frac{C_y-F_y}{F_x-C_x}\cdot y+F_x^2+y^2-2F_yy+F_y^2=k^2$$

Arrange into a quadratic equation - $A\cdot y^2+B\cdot y+C=0$:

$$((\frac{C_y-F_y}{F_x-C_x})^2+1)\cdot y^2+2\cdot((\frac{r^2-k^2+F_x^2+F_y^2-C_x^2-C_y^2}{2\cdot(F_x-C_x)})\cdot(\frac{C_y-F_y}{F_x-C_x})-$$
$$F_x\cdot(\frac{C_y-F_y}{F_x-C_x})-F_y)\cdot y+(\frac{r^2-k^2+F_x^2+F_y^2-C_x^2-C_y^2}{2\cdot(F_x-C_x)})^2$$
$$-2\cdot F_x\cdot(\frac{r^2-k^2+F_x^2+F_y^2-C_x^2-C_y^2}{2\cdot(F_x-C_x)})+F_x^2+F_y^2-k^2=0$$

Extract A, B, C:

$$A=(\frac{C_y-F_y}{F_x-C_x})^2+1$$
$$B=2\cdot((\frac{r^2-k^2+F_x^2+F_y^2-C_x^2-C_y^2}{2\cdot(F_x-C_x)})\cdot(\frac{C_y-F_y}{F_x-C_x})-F_x\cdot(\frac{C_y-F_y}{F_x-C_x})-F_y)$$
$$C=(\frac{r^2-k^2+F_x^2+F_y^2-C_x^2-C_y^2}{2\cdot(F_x-C_x)})^2-$$
$$2\cdot F_x\cdot(\frac{r^2-k^2+F_x^2+F_y^2-C_x^2-C_y^2}{2\cdot(F_x-C_x)})+F_x^2+F_y^2-k^2$$

Solve the quadratic formula:

$$y_{1,2}=\frac{-B\pm\sqrt{B^2-4\cdot A\cdot C}}{2\cdot A}$$

Substitute $y_{1,2}$

$$x_1 = \frac{r^2 - k^2 + F_x^2 + F_y^2 - C_x^2 - C_y^2}{2 \cdot (F_x - C_x)} + \frac{C_y - F_y}{F_x - C_x} \cdot \frac{-B + \sqrt{B^2 - 4 \cdot A \cdot C}}{2 \cdot A}$$
$$x_2 = \frac{r^2 - k^2 + F_x^2 + F_y^2 - C_x^2 - C_y^2}{2 \cdot (F_x - C_x)} + \frac{C_y - F_y}{F_x - C_x} \cdot \frac{-B - \sqrt{B^2 - 4 \cdot A \cdot C}}{2 \cdot A}$$

(34)

2 PCB Schematics

2.1 Wire Combining PCB

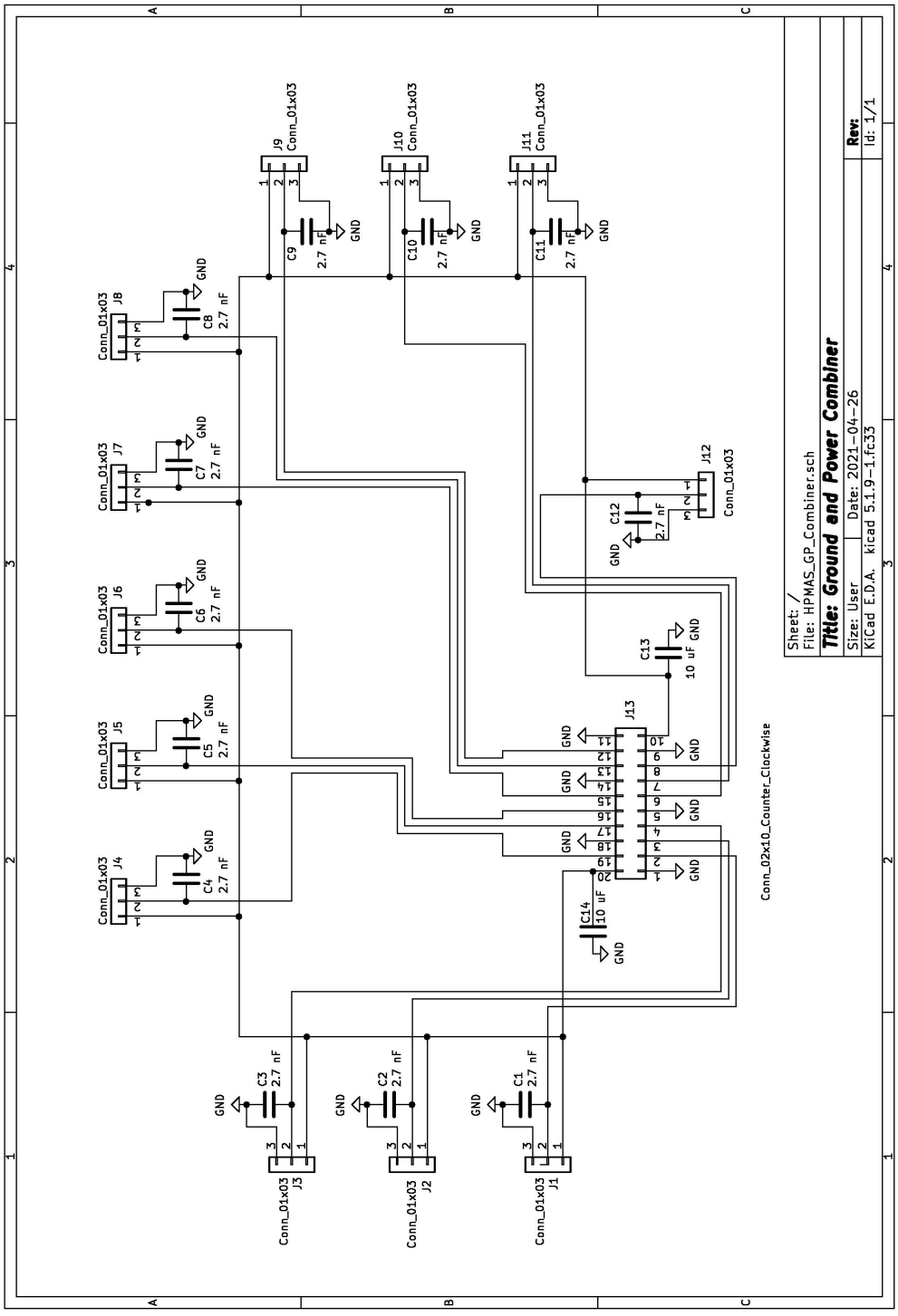

2.2 Multiplexing PCB